THE JOURNAL OF PHYSICAL CHEMISTRY B

Article

pubs.acs.org/JPCB

Catalytic Activity of Human Placental Alkaline Phosphatase (PLAP): Insights from a Computational Study

Gabriela L. Borosky*

INFIQC, CONICET and Departamento de Matemática y Física, Facultad de Ciencias Químicas, Universidad Nacional de Córdoba, Ciudad Universitaria, Córdoba 5000, Argentina

Supporting Information

ABSTRACT: Alkaline phosphatases (APs) catalyze the hydrolysis and transphosphorylation of phosphate monoesters. Quantum-mechanical computational methods were employed to study the catalytic mechanism of human placental AP (PLAP). An active-site model was used, constructed on the basis of the X-ray crystal structure of the enzyme. Kinetic and thermodynamic evaluations were achieved for each reaction step. Calculations shed light on the mechanistic differences that had been experimentally observed between aryl and alkyl phosphates, particularly regarding the rate-determining step. The functional implications of relevant residues in the active site were examined. The present theoretical study rationalizes experimental observations previously reported in the literature.

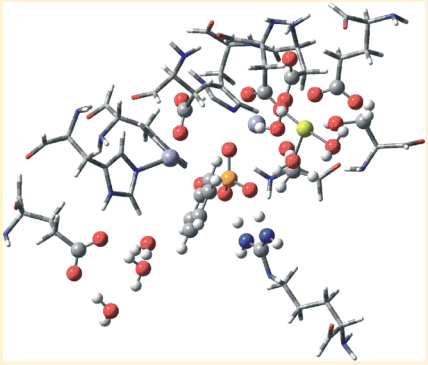

INTRODUCTION

Alkaline phosphatase (AP) superfamily comprises a set of homodimeric metalloenzymes existing in practically all living species.[1] A comparison of selected APs from different organisms has shown that there is 25%−30% conservation of the amino acid sequence, while residues in the active site and surrounding region are completely conserved.[2,3] The amino acid sequence of the mammalian APs has been fit to the structure of the *Escherichia coli* enzyme, further supporting the utility of using the *E. coli* enzyme as a model for all APs.[2] The catalytic mechanism, mainly inferred from structural studies of *E. coli* AP,[4] was thus suggested to be analogous for eukaryotic APs. Three human AP isoenzymes are tissue-specific, comprising placental (PLAP), intestinal (IAP), and germ cell (GCAP), and the fourth one is a nonspecific thermo sensitive AP (TSAP) detected in bone, liver, and kidney.[5]

APs catalyze the hydrolysis and transphosphorylation of diverse phosphate monoesters.[6] The enzymatic mechanism involves formation of a covalent phosphoserine intermediate and release of inorganic phosphate and an alcohol.[6] Inorganic phosphate fills the active-site pocket and is a potent competitive inhibitor of the enzyme. Each active site of the dimeric enzyme comprises three distinct metal binding sites (M1, M2, and M3). The M1 and M2 sites are occupied by zinc ions (also referred to as Zn_1 and Zn_2) that are essential for catalysis.[4] The M3 site contains a magnesium ion that apparently does not play a direct role in the catalytic mechanism, although it has been shown to be important for full activation of the enzyme.[7−10] The hydrogen-bonding network in the active site region and the electrostatic field generated by adjacent amino acid residues promote phosphate stabilization and catalysis.

Kinetic and biochemical studies revealed a two-step reaction mechanism (Scheme 1).[11−13] During the first chemical step, which is generation of the covalent intermediate E-P (k_2, Scheme 1), it is proposed that Zn_2 assists the formation of a more reactive serine alkoxide, whereas Zn_1 is assumed to stabilize the negative charge developing on the leaving group. In the second chemical step, involving hydrolysis of the phosphoserine (k_3, Scheme 1), Zn_1 would activate a water molecule, thus facilitating the generation of a nucleophilic hydroxide ion, and Zn_2 is presumed to stabilize the serine leaving group. In the presence of R_2OH (nucleophilic buffers), transphosphorylation to a phosphate acceptor is shown by k_5.

For aryl phosphates as substrates, the rate-limiting step depends on pH; at acidic pH < 7.5, the hydrolysis of the covalent intermediate E-P (k_3, Scheme 1) is rate-determining, while the release of phosphate from the noncovalent enzyme-phosphate complex ($E.P_i$) (k_4, Scheme 1) turns into the rate-limiting step under basic conditions (pH > 7.5).[14−16] On the other hand, the phosphorylation of the enzyme (k_2) has been indicated as rate-determining for the reaction of alkyl phosphates.[17] *E. coli* AP presents maximum activity at pH 8.[3] In the case of PLAP, optimal activity takes place at pH 10.5, whereas the physiological pH at the placenta surface is approximately 7.[18]

The X-ray crystal structure of PLAP was reported with 1.8 Å resolution (PDB entry 1EW2).[19] One function of PLAP at the placental surface may involve the transfer of maternal IgG to the fetus.[20−22] PLAP has also been deduced to stimulate DNA

Received: September 11, 2014
Revised: November 18, 2014
Published: November 19, 2014

dx.doi.org/10.1021/jp511221c | J. Phys. Chem. B 2014, 118, 14302−14313

Scheme 1. General Catalytic Mechanism of APs

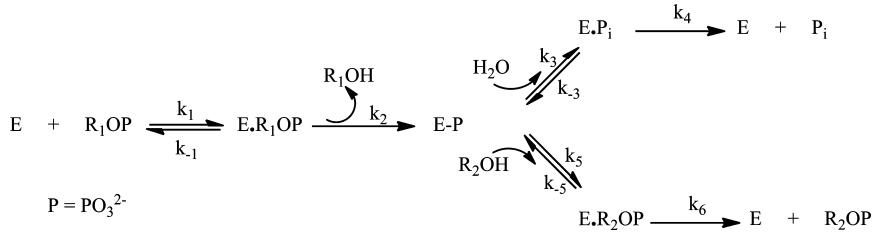

synthesis and cell proliferation in fibroblasts together with insulin, zinc, and calcium ions,[23] and to improve the survival of serum-starved mouse embryos and human fetal fibroblasts.[24] PLAP may also be a significant modulator of fetal growth because increases growth and survival of fetal cells. Furthermore, alterations in PLAP activity have been observed in several diseases, as for example in Chagas' disease.[25] It is one of the proteins ectopically expressed by tumor cells, suggesting the importance of dysregulation of embryonic genes in cancer progression.[26] Additionally, several clinical reports have been published regarding the use of this enzyme as a tumor marker.[27−30] Thus, PLAP is presumed to have a significant role in cancer diagnosis and therapy.

In a previous study, molecular docking, molecular dynamics, and quantum mechanical techniques were employed to study the catalytic mechanism of PLAP.[31] Kinetic and thermodynamic estimations were carried out with methylphosphate as substrate, determining activation barriers and free energy values for each reaction step.[31] The function of Mg^{2+} at the M3 site was analyzed to elucidate its influence on full enzyme activity.[31]

With the aim of achieving further insight into the catalytic activity of PLAP as a particular case, and on the function of the AP superfamily in general, this work presents further molecular docking and quantum chemical calculations on the catalytic mechanism. As a continuation of our prior report,[31] computations for the reaction steps were carried out in this instance with phenylphosphate as the substrate. Comparisons of the observed mechanistic and energetic features were made with the results for methylphosphate. Thus, this study was focused on verifying and explaining the experimental observations reported in the literature concerning the differences in rate-determining step among aryl and alkyl phosphate substrates.[14−17] The roles of the more relevant residues in the active site were also examined.

COMPUTATIONAL METHODS

Docking Procedure. The structure of PLAP was acquired from the Protein Data Bank (PDB code 1EW2).[19] The metal ions (two zinc ions and two magnesium ions) were conserved, and the heteroatoms, including the cofactor and phosphate, were discarded. Crystallographic water molecules were removed, but three molecules completing Mg^{2+} coordination (Wat110 (charge −1 *e*), Wat1, and Wat421) were retained. The program AutoDock 4.2[32] was utilized to carry out automated molecular docking for estimating the interaction energy and modeling the binding modes between PLAP and phenylphosphate dianion. Addition of hydrogens, merger of nonpolar hydrogens to the atom to which they were linked, and assignation of partial charges to PLAP atoms were achieved with AutoDockTools. Merz−Kollman partial atomic charges were employed for PLAP, and Gasteiger charges were assigned to phenylphosphate dianion (for a discussion on selection of charge types, see ref 31). Except for zinc-coordinated histidines (His320, His432, His358), which were singly protonated on Hδ, all other histidines were treated as neutral, singly protonated on Hε. The side chains of arginine, lysine, aspartate, and glutamate residues were considered as ionized. The docking area within the active site of PLAP was defined with the AutoGrid module in AutoDock. The grid site was constricted to a 23.62 Å cubic space centered on the original phosphate group present in the crystal structure.[19] The grid box, including the whole binding site of PLAP, provided proper space for rotational and translational movement of the phenylphosphate ligand. The conformational and orientational spaces of the ligand and flexible residues Ser92 and Arg166 were searched, whereas the other amino acids were rigid. The Lamarckian genetic algorithm (LGA) was used, default parameters were applied, and the maximum number of energy evaluations was set to 1.0×10^7. For each of the 100 independent runs performed, a maximum number of 2.7×10^4 genetic algorithm operations were generated on a single population of 150 individuals. Operator weights for crossover, mutation, and elitism were default parameters, 0.80, 0.02, and 1, respectively.

General Methodology for Quantum-Chemical Calculations. Procedures were based on the cluster approach, which has been successfully applied to modeling enzymatic reactions.[33−35] In this method, a limited part of the enzyme is properly selected to represent the active site at a quantum mechanic level, usually by using a DFT functional. The rest of the protein not explicitly included surrounding the active site may influence the model in two major respects. First, by causing steric constraints, which, if not considered, could lead to substantial artificial movements of the model residues, because the geometry would change as a result of the lack of surrounding amino acids. Hence, certain crucial coordinates at the boundary of the model are kept rigid from available X-ray structures to model the steric effects. Also, the positions of the backbone atoms are fixed when obtained from high-resolution X-ray structures, while the coordinates of the rest of the atoms are optimized. Second, the polarization caused by the enzyme surroundings can influence the calculated energies, therefore polarizable continuum techniques are generally used to consider the electrostatic effects. Solvation energies are obtained from single-point calculations of the optimized geometries with a dielectric constant $\varepsilon = 4$ to represent the protein environment.[33−35] It has been verified that relative solvation effects decrease very quickly as the model size grows, since more groups providing polarization are explicit. This combination of a coordinate-locking procedure and continuum solvation efficiently accounts for the residues not included in the model, yielding suitably accurate computed energies.[33−35]

QM/QM-ONIOM computations were carried out in this work with a model consisting of 219 quantum atoms, a model

dx.doi.org/10.1021/jp511221c | J. Phys. Chem. B 2014, 118, 14302−14313

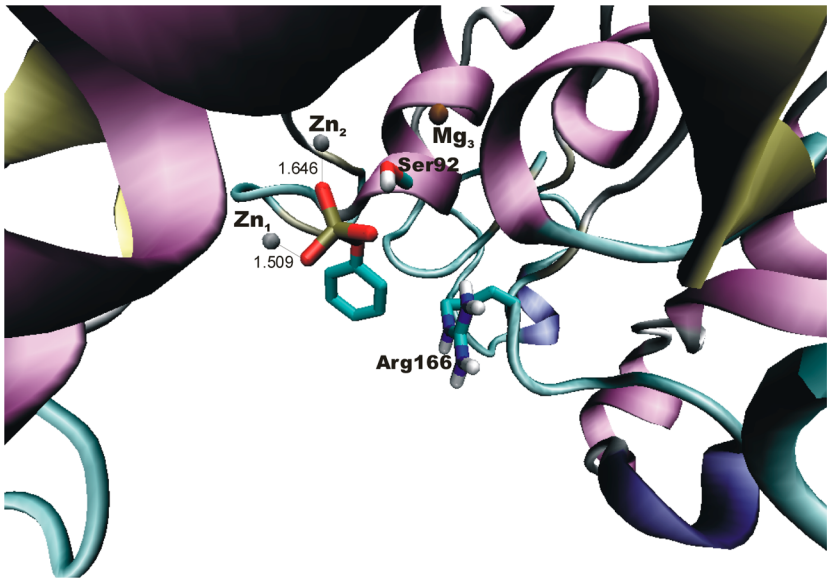

Figure 1. Best docked conformation of phenylphosphate dianion in the crystal structure of PLAP.

size that is assumed to afford precise results by the cluster method.[33−35] The starting geometry was built from an X-ray structure with an atomic resolution of 1.8 Å (PDB entry 1EW2).[19] Prior MD simulations confirmed the stability of the crystal structure, specifically within the active site region.[31] The coordinates of the backbone atoms were kept fixed to avoid deformation of the active site during geometry optimization, and the side chains of all residues were relaxed, as this procedure has been previously proved to be valid.[31] The influence of the environment was considered by means of a polarizable implicit continuum solvation model using a dielectric constant $\varepsilon = 4.0$ to represent the residues surrounding the active site.

Enzyme Model. The three-dimensional structure of PLAP was obtained from the Protein Data Bank (PDB code 1EW2).[19] Both Zn^{2+} ions (M1 and M2) and one Mg^{2+} ion (M3) were selected as well as their ligands: Asp316, His320, His432, His358, Asp357, Asp42, Glu311, Ser155, nucleophilic Ser92, and the important residues Arg166 and Glu429 (hydrophilic pocket).[19] Valence at cut peptide bonds were completed with hydrogens. Six water molecules were also retained: three to complete Mg^{2+} coordination (one as a hydroxide ion), and three close to Glu429. The phosphate ion in 1EW2 was utilized as a template of the monoester substrate phenylphosphate dianion (charge -2 e). The side chains of arginine, aspartate, and glutamate residues were considered as ionized, and histidines were defined as neutral, singly protonated on Hδ. The complete model system had a net charge of -1, resulting from the sum of seven positive charges (two Zn^{2+} cations, one Mg^{2+}, and one arginine) and eight negative charges (three aspartates, two glutamates, one hydroxide anion, and phenylphosphate dianion).

Quantum-Mechanical Methods. Two-layer QM/QM-ONIOM[36] calculations were performed with the Gaussian 09 package of programs.[37] Density Functional Theory (DFT) optimizations with the B3LYP[38−40] and ωB97X-D[41] functionals were carried out for the high layer, consisting of the three metal cations, phenylphosphate dianion, five water molecules, one hydroxide ion, carboxylate groups of glutamates and aspartates, $-CH_2OH$ groups of serines, and the $-C(NH_2)_2$ group of arginine (42 heavy atoms and 26 hydrogens). The 6-31+G* basis was employed for C, O, N, P, Mg, and H atoms, and the pseudopotential Lanl2DZ was utilized for Zn. For the low layer (73 heavy atoms and 78 hydrogens), minimizations with the semiempirical PM3MM[42] and PM6[43] methods were performed. The positions of the backbone atoms (implicated in peptide bonds) were fixed to preserve the active site structure, while positions of all the other atoms were fully optimized. Minima and transition states (TSs) on the potential energy surface were characterized by means of harmonic vibrational frequency calculations, which also provided zero-point vibrational energies, thermal corrections, enthalpies, entropies, and free energies. The electrostatic effect of the environment was considered via polarized continuum model (IEFPCM)[44−47] single-point energy computations on the optimized stationary points, by using a dielectric constant $\varepsilon = 4.0$ to simulate the influence of the residues surrounding the active site.

RESULTS AND DISCUSSION

Molecular Docking. The 100 docking modes of phenylphosphate dianion within PLAP produced three clusters. Phenylphosphate dianion presented a favorable $\Delta G_{binding} = -9.58$ kcal/mol, this binding affinity corresponding to the lowest energy mode of the best docked and most populated cluster, which presented 47 poses clustered within 2 Å RMSD. Strong coordination with Zn_1 and Zn_2 was observed (Figure 1). The major contribution to the binding energy was electrostatic (-11.32 kcal/mol), and the sum of van der Waals interactions, hydrogen bonding, and desolvation yielded 1.14 kcal/mol.

Quantum-Chemical Calculations. The active site of PLAP comprises the catalytic Ser92, the metal triplet (two Zn^{2+} and one Mg^{2+}), Arg166, Glu429, and some proximate residues (Figure 2). The hydrophilic pocket composed by Arg166 and Glu429 is thought to stabilize the hydrophilic part of the phosphate monoester ligand. Additionally, Glu429 also stabilizes the water molecules, bridging the gap to the phosphate group of the phosphoseryl intermediate.[48] One of these waters is significantly retained and implicated in the nucleophilic attack on the phosphoserine. In addition, several

dx.doi.org/10.1021/jp511221c | J. Phys. Chem. B 2014, 118, 14302−14313

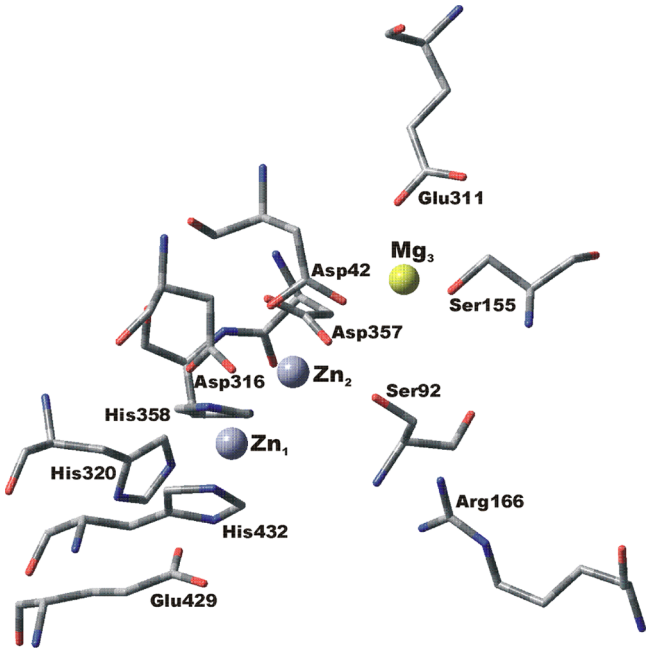

Figure 2. Active site of PLAP with the relevant neighboring amino acids.

water molecules are located within the active site and form an extensive hydrogen-bonding network.

Phenylphosphate Substrate. The catalytic mechanism (Scheme 2) was modeled inside the active site from the Michaelis complex. The preliminary structure for the covalent complex was constructed from the molecular docking results (Figure 1). The phenylphosphate ligand was rotated to promote the nucleophilic attack from Ser92. In this orientation, the oxygen from the ester leaving group was coordinated to Zn_1, one nonbridging oxygen was coordinated to Zn_2, and the other two nonbridging oxygen atoms were hydrogen-bonded with the guanidinium group of Arg166.

In the optimized geometry for the Michaelis complex (Figure 3a), Zn_1 was tetracoordinated with the imidazole nitrogen atoms of His320 and His432, one carboxyl oxygen of Asp316, and the esteric oxygen of the phosphate substrate. Metal–ligand bond distances were in the range between 1.99 and 2.24 Å with the ONIOM(B3LYP:PM3MM) scheme, and between 1.83 and 2.01 Å for the ONIOM(ωB97X-D:PM6) geometry optimization. Zn_2 was pentacoordinated by one carboxyl oxygen of Asp357 and Asp42, the hydroxyl of Ser92, the imidazole nitrogen atom of His358, and one nonbridging oxygen of the phosphate, the average metal–ligand distance being 2.10 Å. Mg_3 was octahedrally hexacoordinated with the second carboxyl oxygen of Asp42, one carboxyl oxygen of Glu311, the hydroxyl of Ser155, and three water molecules, building a slightly distorted tetragonal bipyramid with a mean Mg–O distance of 2.11 Å. The water molecule originally included as a hydroxide ion became protonated by the hydroxyl group of Ser92 after energy minimization. In this way, the catalytic serine turned to its ionized form. This spontaneous proton transfer was also observed in our previous work,[31] and it had been suggested in the literature.[4,17,49] The two other nonbridging oxygens of phenylphosphate dianion were hydrogen bonded to the nitrogen atoms of the guanidinium group of Arg166. One of these oxygens was also hydrogen bonded to one water molecule from the coordination shell of Mg_3, as it has been suggested.[50] These stabilizing interactions of the nonbridging phosphate oxygens (with Zn_2, Arg166, and one Mg_3-bound water) remained throughout the mechanistic pathway.

The covalent phosphoserine intermediate was subsequently formed (Scheme 2, Step 1). The phenoxide leaving group was stabilized by coordination to Zn_1. Phenoxide anion was displaced from metal coordination by one water molecule in Step 2. A Zn_1-coordinated hydroxide ion was formed in Step 3. With methoxide as the leaving group,[31] this proton transfer yielded methanol. However, the hydroxide/phenol configuration could not be characterized in this case, as the system spontaneously returned to the original water/phenoxide pair; this behavior can be explained by considering the pK_as involved (pK_a H_2O = 15.7, pK_a MeOH = 15.5, pK_a PhOH = 10.0).[51] Instead, the nucleophilic hydroxide was obtained by transferring the proton to the more distant Glu429. In Step 4, hydroxide attacked the phosphoserine, releasing a hydrogen phosphate dianion and regenerating the nucleophilic serine

Scheme 2. Hydrolytic Mechanism for Phenylphosphate Dianion by PLAP

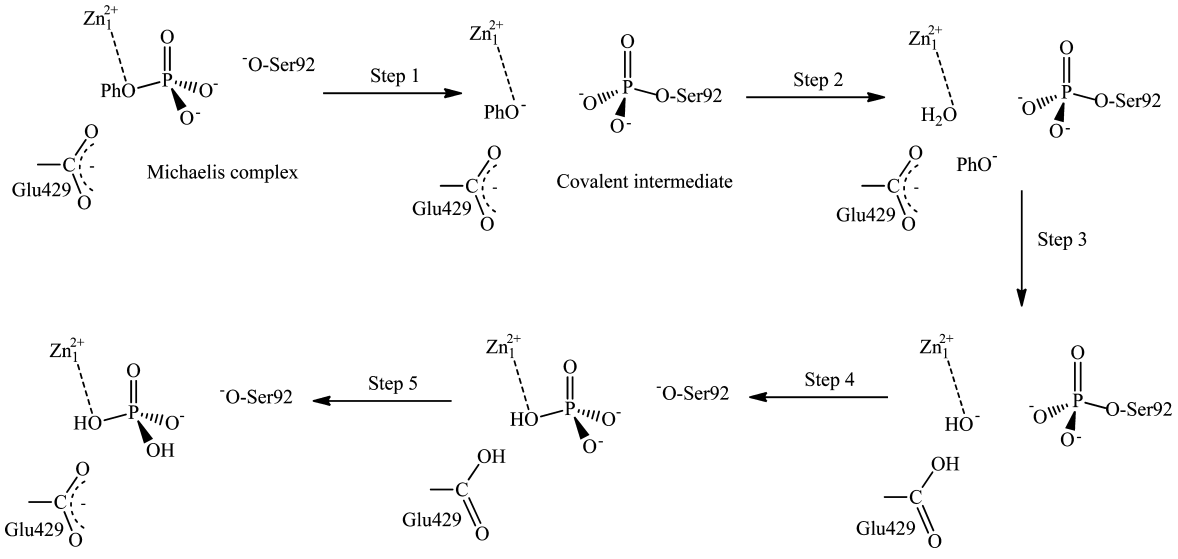

dx.doi.org/10.1021/jp511221c | J. Phys. Chem. B 2014, 118, 14302–14313

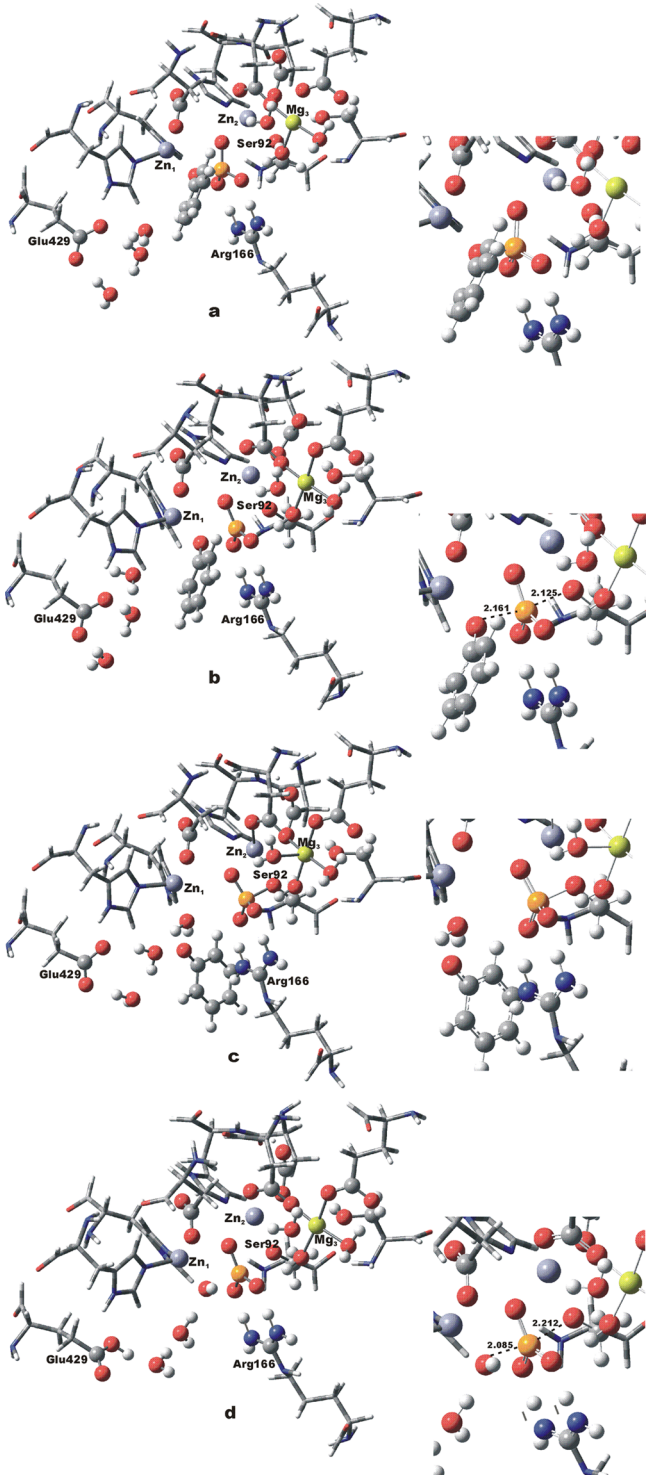

Figure 3. Selected stationary points of the catalytic mechanism. (a) Michaelis complex. (b) TS for serine nucleophilic attack (bond distances in Å). (c) Covalent phosphoserine intermediate, water complexed to Zn_1. (d) TS for phosphoserine hydrolysis (phenoxide anion has left, bond distances in Å).

oxyanion. In Step 5, a proton transfer from Glu429 returned this residue to its initial ionized form, generating dihydrogen phosphate ion as the final product of the mechanism. The structures for some selected stationary points are shown in Figure 3, while energies are presented in Table 1. In general, solvation effects were relatively small, indicating that the protein model employed accounted for most polarization.[52] Reaction free energy profiles are illustrated in Figure 4.

The TS for the first chemical step, involving generation of the covalent phosphoserine (Step 1, Scheme 2), presented a trigonal bipyramidal configuration (Figure 3b) corresponding to an in-line displacement reaction, as proposed by Holtz et al.[53] The distance between phosphorus and the nucleophilic oxygen of serine was 2.125 Å with B3LYP (2.058 Å with ωB97X-D), and the bond length from phosphorus to the oxygen of the phenoxide leaving group was 2.161 Å by B3LYP (2.101 Å with ωB97X-D). Bond forming/breaking oxygens were in an opposite axial disposition forming an angle of approximately 171 degrees. The three nonbridging oxygens of the transferred phosphoryl group, separated by nearly 120 degrees, bisected the axial plane forming stabilizing interactions with Arg166, Zn_2, and one Mg_3-bound water. Departure of the phenoxide leaving group was assisted by coordination with Zn_1. The noncovalent complex converted into the covalent phosphoserine through a small rotation of the side chain of Ser92. The positions of the other residues experienced only minor changes, denoting the optimal configuration of the active site for stabilizing the transition structure.

The nucleophilic attack of a hydroxide anion coordinated to Zn_1 on the phosphoseryl intermediate (second chemical step, Step 4, Scheme 2), presented also a trigonal bipyramidal TS (Figure 3d) corresponding to another in-line displacement. The bond length from phosphorus to the oxygen of the hydroxide nucleophile was 2.085 Å with B3LYP (2.015 Å with ωB97X-D), and the distance between phosphorus and the oxygen atom of the leaving serine was 2.212 Å by B3LYP (2.204 Å with ωB97X-D). This transition structure presented stabilizing interactions of the phosphoryl group similar to those observed in the first TS, and only minimal variations were found in the atomic coordinates of the model residues, evidencing the assistance of the active site structure to the catalytic mechanism.

It is worth mentioning that the interatomic distances between the three metal cations were reasonably conserved through the whole mechanism displayed in Scheme 2, even though their positions were allowed to move freely during the optimization process. Thus, the Zn_1-Zn_2 and Zn_2-Mg_3 distances always fluctuated around 4 Å, whereas the Zn_1-Mg_3 distance remained close to 7 Å, the values observed in the crystal structure.[19] Conservation of the distances between the metal ions has been remarked to be important when considering the accuracy of calculations on this type of reactions catalyzed by the alkaline phosphatase superfamily of enzymes.[54,55] On considering the density functionals employed, it should be noticed that B3LYP turned out to be more efficient than ωB97X-D in locating stationary points, especially in the case of TSs.

M3-Zn Enzyme Model. It has been suggested that a Mg^{2+}-bound hydroxide ion acts as a general base to deprotonate the nucleophilic serine.[4,17,49] However, more recent observations are inconsistent with a general base catalysis model and propose that the transferred phosphoryl group is indirectly stabilized in the TS by the Mg^{2+} ion through a coordinated water ligand.[50] In order to evaluate the effect of the magnesium ion at the M3 site of the wild-type enzyme, computations for the mechanism in Scheme 2 were repeated with an enzyme model where the Mg^{2+} in M3 was replaced by Zn^{2+}.

The optimized structure of the Michaelis complex ending up being similar to the one found with magnesium at M3. The average Zn−O bond length was 2.15 Å, somewhat greater than

dx.doi.org/10.1021/jp511221c | J. Phys. Chem. B 2014, 118, 14302−14313

Table 1. Changes in Reaction and Activation Free Energies Computed for the Hydrolysis of Phenylphosphate and Methylphosphate Dianions by PLAP[a]

		calculations at the ONIOM(B3LYP:PM3MM) level [ONIOM(ωB97X-D:PM6) level] (kcal/mol)[b]						
		Step 1		Step 2	Step 3	Step 4		Step 5
substrate	protein	ΔG_r	$\Delta G^{\ddagger}$	ΔG_r	ΔG_r	ΔG_r	$\Delta G^{\ddagger}$	ΔG_r
phenylphosphate	wild-type enzyme (M3-Mg)	6.1	10.5	−16.8	16.8	1.8	12.4	−11.9
		(0.5)	(10.0)	(−6.9)	(13.1)	(4.3)	(13.5)	(−11.5)
		[1.9]	[4.8]	[−7.5]	[13.0]	[9.7]	[12.2]	[−6.4]
		([−2.5])	([5.4])	([−0.7])	([9.9])	([14.7])	([16.0])	([−15.5])
	M3-Zn	5.6	8.1	−26.8	14.0	9.1	31.5	−6.5
		(2.8)	(8.9)	(−18.3)	(15.3)	(14.3)	(25.3)	(−9.0)
		[3.4]	[10.5]	[−8.4]	[9.7]	[17.3]	[29.1]	[−26.5]
		([−1.7])	([8.0])	([0.0])	([11.1])	([15.1])	([28.6])	([−21.6])
methylphosphate	wild-type enzyme (M3-Mg)	18.3	22.0	−12.2	3.8	−27.0	1.8	-
		(16.8)	(20.6)	(−9.6)	(2.2)	(−17.5)	(3.1)	
		[20.2]	[21.6]	[−4.4]	[−5.6]	[−14.9]	[3.0]	
		([12.6])	([15.4])	([2.5])	([−9.5])	([−6.6])	([9.2])	
	M3-Zn	18.1[c]	21.6[c]	−21.4[c]	5.5[c]	−10.3[c]	5.5[c]	-
		(13.4)	(14.9)	(−14.6)	(1.2)	(−8.7)	(7.5)	

[a]Reaction steps are displayed in Schemes 2 and 3. [b]IEFPCM single-point results in parentheses. [c]From ref 31.

for Mg. The covalent phosphoserine was also analogous to the one characterized with the wild-type model. Accordingly, the first chemical step afforded similar changes in free energies of reaction and activation when a Mg or a Zn cation was present at M3 (Table 1).

Displacement of methoxide ion from Zn_1 coordination by a water molecule (Step 2, Scheme 2) produced a change in the conformation of the M3 site and Zn_3 became pentacoordinated, forming a distorted square pyramid after loss of coordination to Ser155 (Supporting Information, Figure S1). This outcome is presume to arise from the tendency of Zn^{2+} for presenting tetrahedral over octahedral coordination.[56] This variation of the active site structure produced a stronger phosphoserine bond of 1.708 Å vs 1.756 Å in the wild-type model with B3LYP (1.680 Å vs 1.734 Å by ωB97X-D). At the same time, the phosphoryl group became stabilized by a second hydrogen bond interaction with another Zn_3-bound water molecule. Furthermore, an increment in the distance between phosphorus and the nucleophilic Zn_1-coordinated water molecule was observed (3.688 Å vs 3.487 Å in the wild-type enzyme by B3LYP, 3.582 Å vs 3.408 Å with ωB97X-D), along with a displacement of the phosphoserine to a less favorable position for the next hydrolytic Step 4 (from an OPO angle of about 170 degrees in the wild-type enzyme to around 150 degrees). Pentacoordination of Zn_3 was kept in the following steps. These modifications generated a more exothermic displacement from Zn_1-coordination for the methoxide anion (Step 2), and a higher activation free energy for the hydrolysis of the phosphoserine (Step 4) for the M3-Zn protein according to the B3LYP results (Table 1, Figure 4b). On the other hand, ωB97X-D yielded a similar exothermicity for Step 2, but a higher barrier for Step 4 (Table 1, Figure 4c). Nevertheless, both density functionals indicated a lower activity for the M3-Zn mutant, in accordance with the known experimental observations.[7−10] It is interesting to note that in the TS for hydrolysis of the covalent phosphoseryl intermediate (Step 4), one of the nonbridging oxygens of the phosphoryl group became directly coordinated to Zn_3 (displacing Glu311 from the coordination shell), while conserving a hydrogen bond interaction with one Zn_3-bound water.

The final product was hydrogen phosphate dianion, as the proton transferred from Glu429 protonated Ser92. In this way, the nucleophilic residue rotated its side chain to form a hydrogen bond with Asp357. Zn_3 resulted pentacoordinated by Ser92, Ser155, one oxygen atom of Asp42, and two water molecules. The third water, now excluded from the Zn_3 coordination shell, was hydrogen bonded to one nonbridging oxygen of the phosphate product. As phosphate is known to produce inhibition of the enzyme by hindering k_4 (Scheme 1),[17] this extra stabilization of the final product could also be implicated in the lower activity of the M3-Zn mutant.

Methylphosphate Substrate. The catalytic mechanism of PLAP with methylphosphate as substrate has been recently modeled by ONIOM(B3LYP:PM3MM) calculations in our former study.[31] Now, computations were repeated with the ONIOM(ωB97X-D:PM6) scheme for comparison purposes. However, results reported in ref 31 consisted of gas-phase computations on the same enzyme model as this work, and IEFPCM calculations on a reduced model system. Hence, the present IEFPCM values in Table 1 for the largest enzyme model correspond to new results. It should be noticed that, with methoxide anion as the leaving group, it was feasible to model the proton transfer from the Zn_1-coordinated water to generate methanol and hydroxide ion. Therefore, the calculated mechanism for this substrate is shown in Scheme 3. Calculations were conducted with the wild-type model as well as with the M3-Zn mutant. Reaction free energy profiles are displayed in Figure 5.

Geometries of the stationary points at the ONIOM(ωB97X-D:PM6) level resulted very similar to the ones described in ref 31. Zn−ligand bond distances optimized with ONIOM-(ωB97X-D:PM6) were ca. 0.2 Å shorter than the corresponding ONIOM(B3LYP:PM3MM) values, as described for the phenylphosphate case. In the TS for Step 1, the bond length between P and the nucleophilic oxygen of serine was 2.106 Å with ωB97X-D (1.933 Å by B3LYP[31]), whereas the distance from P to the oxygen of the methoxide leaving group was 1.898 Å with ωB97X-D (2.336 Å by B3LYP[31]). For the second TS (Step 4), the bond distance between P and the oxygen of the hydroxide nucleophile was 2.312 Å with ωB97X-D (2.513 Å

dx.doi.org/10.1021/jp511221c | J. Phys. Chem. B 2014, 118, 14302−14313

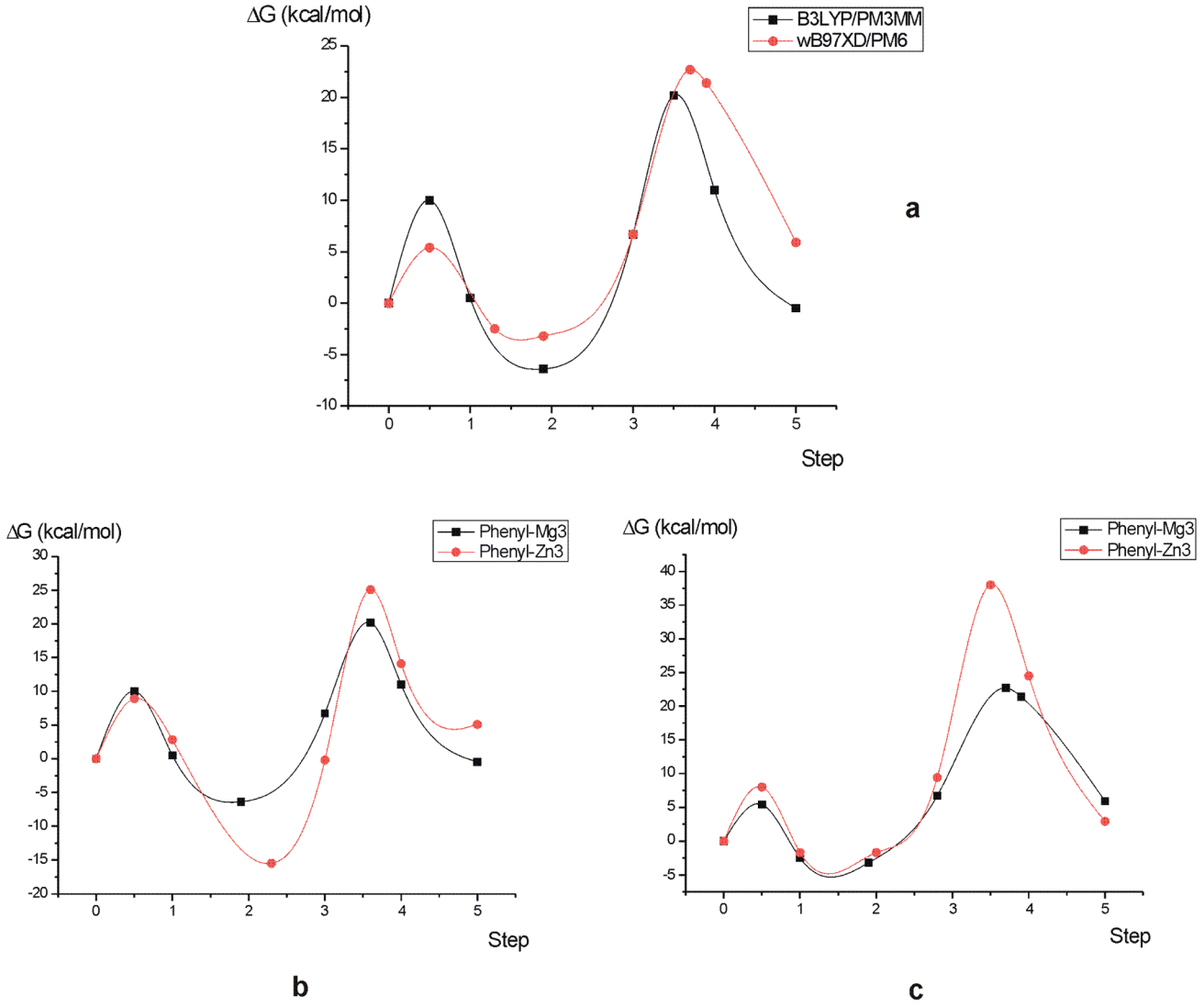

Figure 4. Free energy profiles for the reaction of phenylphosphate dianion (IEFPCM single-point results). (a) Comparison between results with different density functionals. (b) Comparison between the wild-type model and the M3-Zn protein with the ONIOM(B3LYP:PM3MM) scheme. (c) Comparison between the wild-type enzyme and the M3-Zn mutant with ONIOM(ωB97X-D:PM6).

Scheme 3. Hydrolytic Mechanism of Methylphosphate Dianion by PLAP

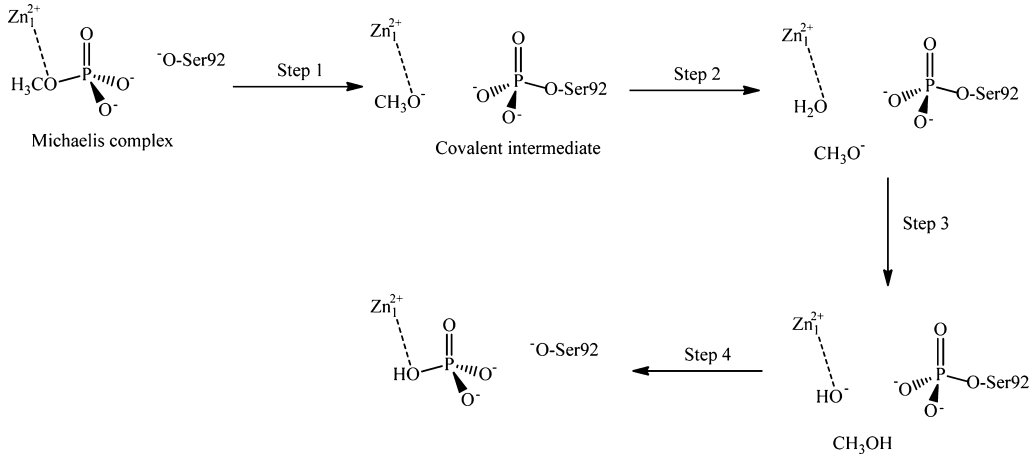

with B3LYP[31]), and the distance from P to the oxygen of the leaving serine was 1.911 Å with ωB97X-D (1.898 Å by B3LYP[31]).

With the M3-Zn model protein, computational results were consistent with those reported in ref 31. A change in the configuration of the M3 site was also observed upon

dx.doi.org/10.1021/jp511221c | J. Phys. Chem. B 2014, 118, 14302−14313

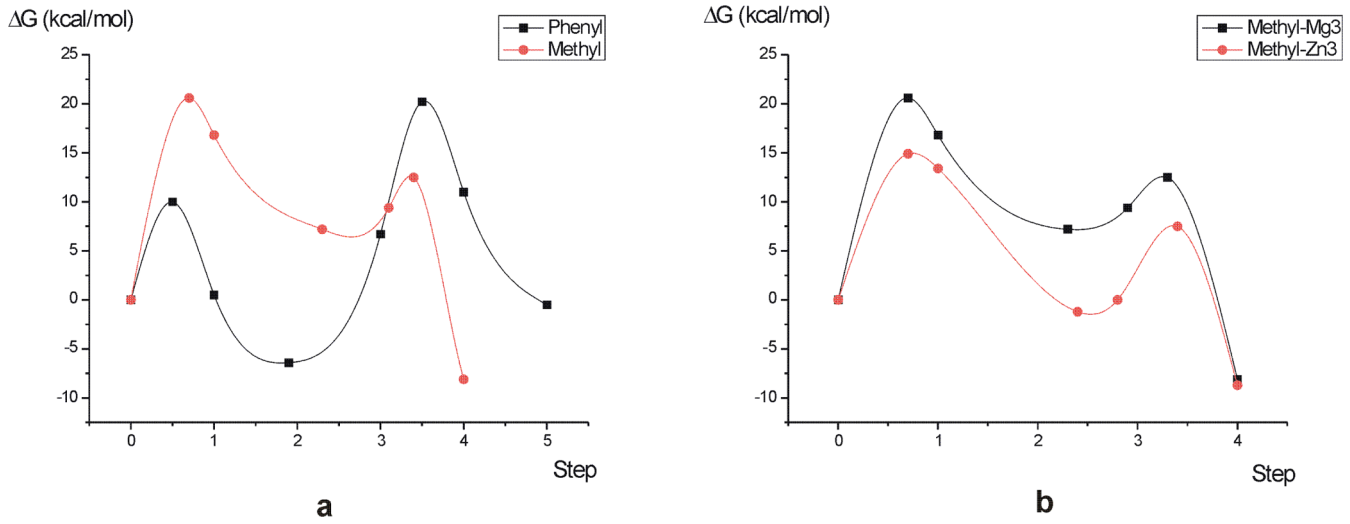

Figure 5. ONIOM(B3LYP:PM3MM) free energy profiles for the reaction of methylphosphate dianion (IEFPCM single-point results). (a) Comparison between results for phenylphosphate and methylphosphate as substrates. (b) Comparison between the wild-type model and the M3-Zn protein for methylphosphate.

displacement from Zn_1 coordination of methoxide ion by a water molecule (Step 2, Scheme 3). Thus, Zn_3 resulted pentacoordinated by one oxygen of Asp42, three water molecules, and one of the nonbridging oxygens of the phosphoryl group. This distorted square pyramid configuration of the Zn_3 coordination shell was conserved during the following steps of the catalytic mechanism. This change in the active site configuration lowered the free energy profile for hydrolysis of the phosphoserine intermediate. In contrast, the larger stabilization of the phosphoseryl group, probably originated by complexation of one of the phosphate oxygens with Zn_3, provoked a slight increase in the free energy of activation for hydrolysis of the phosphoserine (Table 1, Figure 5b).

Kinetic Considerations. According to the values in Table 1, transition-state theory[57] was employed to determine the corresponding rate constants (nomenclature for rate constants corresponds to the general mechanism in Scheme 1). For phenylphosphate as the substrate, kinetic parameters were as follows: for the chemical step 1, $k_2 = 2.9 \times 10^5$ s^{-1} by B3LYP, and 6.8×10^8 s^{-1} with ωB97X-D ($\Delta G^{\ddagger}$ = 10.0 and 5.4 kcal/mol, respectively); and for chemical step 4, $k_3 = 7.9 \times 10^2$ s^{-1} with B3LYP, 11.6 s^{-1} with ωB97X-D ($\Delta G^{\ddagger}$ = 13.5 and 16.0 kcal/mol, respectively). These values indicate that the hydrolysis of the covalent intermediate (k_3) is the rate-limiting step of the catalytic mechanism for phenylphosphate monoester. On the other hand, for the methylphosphate substrate the computed values resulted: $k_2 = 4.9 \times 10^{-3}$ s^{-1} (B3LYP), and 31.9 s^{-1} (ωB97X-D), with $\Delta G^{\ddagger}$ = 20.6 and 15.4 kcal/mol, respectively; $k_3 = 3.3 \times 10^{10}$ s^{-1} (B3LYP), and 1.1×10^6 s^{-1} (ωB97X-D), $\Delta G^{\ddagger}$ = 3.1 and 9.2 kcal/mol, respectively, pointing out the nucleophilic attack of the serine alkoxide to phosphorus as the rate-determining step for this alkyl phosphate. Although for aryl phosphates the rate-determining step at pH > 7.5 corresponds to product release (k_4), and to the hydrolysis of the phosphoserine (k_3) at pH < 7.5,[14−16] phosphorylation of the enzyme (k_2) has been indicated as rate-limiting for alkyl phosphates.[17] Hence, the present computational results for both types of substrates are in good agreement with the mechanistic features derived from experimental measures.

Even though hydrolysis of the phosphoserine is the same reaction for both substrates (Step 4 in Schemes 2 and 3), the activation barrier for this step turned out to be considerable lower with methylphosphate than for phenylphosphate. Moreover, this reaction was exothermic for methylphosphate, but endothermic with the aromatic substrate (Table 1). These facts were reflected in the respective TS structures, being of earlier nature for methylphosphate than for phenylphosphate (see relevant bond lengths described above for both TSs). It should be noticed that the model system was the same for both substrates, but the total charge was −1 *e* after departure of methanol in Step 3 (Scheme 3), while the system became neutral after removal of phenoxide (Scheme 2). It has been shown that activation energies for phosphoryl transfer reactions in metalloenzymes are very sensitive to the charge balance around the active center, and that a neutral model is more suitable for reproducing experimental data.[58] Nevertheless, the present calculations indicate that the feasibility of the proton transfer that generates the HO^- nucleophile (Step 3 in Schemes 2 and 3) is an important factor in determining the hydrolysis of the phosphoserine (k_3) as the rate-limiting step at pH < 7.5 for aromatic phosphates. The zinc-coordinated water molecule has been suggested to have a pK_a of 8.0.[17]

Since the experimental rate constants for the noncatalyzed hydrolysis reactions of methylphosphate and phenylphosphate dianions in water at 25 °C are $k_{exp} = 2 \times 10^{-20}$ s^{-1}, and 3×10^{-14} s^{-1}, respectively,[59] the present computations denote that PLAP increases the reaction rate by a factor of 2.4×10^{17} with methylphosphate as the substrate, and of 2.6×10^{16} for phenylphosphate (B3LYP calculations). These observations are in good accordance with the catalytic proficiencies experimentally measured for APs.[60]

Computational results get actual validation when compared with experimental measurements. In this way, reproduction of experimental observations is an appropriate test of the precision and applicability of theoretical methods, and for supporting the interpretations derived from them, as well as their predictive capability. Comparison of theoretical and experimental kinetic data is not direct. Calculated barriers correspond to the free energy difference between the TS and the Michaelis complex ($\Delta G_{cat}^{\ddagger}$), and are related to k_{cat}. On the other hand,

dx.doi.org/10.1021/jp511221c | J. Phys. Chem. B 2014, 118, 14302−14313

Table 2. Comparison between Experimental and Computed Kinetic Parameters for the Chemical Steps of the Catalytic Mechanism (Wild-Type Enzyme): Activation Free Energies ($\Delta G^{\ddagger}$ (kcal/mol)), and Rate Constants at 25°C (k_{cat}/K_M ($M{\cdot}s^{-1}$) or k_{cat} (s^{-1}) for Experimental Values; k_{cat} (s^{-1}) for Calculated Values)[a]

		substrate			
		phenylphosphate		methylphosphate	
reaction step	kinetic parameter	experimental values[b]	calculated values[c]	experimental values[b]	calculated values[c]
1	$\Delta G^{\ddagger}$	<13.4[d]	10.0 [5.4]	9.2[e]	20.6 [15.4]
	k_2	$>10^3$ s^{-1}[d]	2.9×10^5 [6.8×10^8]	1.2×10^6 $M{\cdot}s^{-1}$[e]	4.9×10^{-3} [31.9]
4	$\Delta G^{\ddagger}$	7.4[e] ~16.2[f]	13.5 [16.0]	~16.2[f]	3.1 [9.2][g]
	k_3	2.4×10^7 $M{\cdot}s^{-1}$[e] ~0.6 s^{-1}[f]	7.9×10^2 [11.6]	~0.6 s^{-1}[f]	3.3×10^{10} [1.1×10^6][g]

[a]Reaction steps are illustrated in Schemes 2 and 3, and nomenclature for rate constants corresponds to Scheme 1. [b]Assays performed at 25 °C, pH 8.0. [c]At the ONIOM(B3LYP:PM3MM) level (ONIOM(ωB97X-D:PM6) results in brackets), 25 °C. [d]From ref 61. [e]From ref 17. [f]Estimated from ref 62. [g]By using a neutral active site model, values are the same as for phenylphosphate (see text).

experimentally reported values are k_{cat}/K_M, which provide the free energy barrier as measured from the ground state of the free enzyme and substrate in solution to the TS for the first irreversible reaction step ($\Delta G_E^{\ddagger}$). Both free energy barriers are related through the binding free energy of the substrate ($\Delta G_E^{\ddagger} = \Delta G_{cat}^{\ddagger} - \Delta G_{Binding}$). Therefore, the experimental k_{cat}/K_M value gives $\Delta G_E^{\ddagger}$ as a lower bound for the calculated free energy of activation of a chemical step ($\Delta G_{cat}^{\ddagger}$). In line with this, k_{cat}/K_M corresponds to a higher limit for k_{cat}. Table 2 summarizes kinetic parameters from experimental studies reported in the literature, along with the corresponding values obtained by the present computations.

As shown in Table 2, computations fairly agreed with the available experimental assessments. Calculated activation barriers turned out to be higher than those derived from k_{cat}/K_M values, and consistent with those derived from k_{cat} measures, supporting the reliability of the level of theory and computational methodology employed in this work. For phenylphosphate as substrate, it is worth noting the very good accordance for the activation free energy of hydrolysis of the covalent intermediate, determined as 16.2 kcal/mol by measuring the breakdown of a radioactive E-P complex (k_3),[62] and the estimations afforded by both density functionals (13.5 kcal/mol with B3LYP, 16.0 kcal/mol for ωB97X-D) (in the methylphosphate case, a difference in the total charge of the protein model have been discussed above). For alkyl phosphates, phosphorylation of the enzyme should have a barrier higher than 16.2 kcal/mol, as experimental evidence have suggested k_2 as rate-limiting.[17] The present B3LYP results, which yielded a barrier of 20.6 kcal/mol, are in accordance with this observations.

In a very recent DFT study, methyl and *p*-nitrophenylphosphate dianions were used as substrates for modeling the hydrolysis of alkyl and aryl phosphates, employing an enzyme model very similar to the one described in the present work.[63] For methylphosphate, energy barriers of 16 kcal/mol were obtained for both chemical steps. Underestimation of the first barrier could have been caused by the lack of diffuse functions in the basis set utilized for geometry optimizations. Diffuse functions are required to adequately describe structural and energetic properties of anionic species, due to the weakly bound nature of the extra electrons.[64]

Comparison of the potential energy surfaces calculated for both substrates (Table 1, Figure 5a) allows gaining insight into the factors determining the change in rate-limiting step between alkyl and aryl phosphates. The difference in basicity between the corresponding leaving groups appears to be the main feature influencing the barrier height for the first chemical step (k_2). Hence, departure of the more stable phenolate anion is the thermodynamically preferred process, involving an earlier TS of lower energy. Regarding the second chemical step (k_3), the presence of the more basic methoxide anion would promote ionization of the Zn_1-coordinated water molecule to generate the nucleophilic hydroxide, facilitating the hydrolysis of the phosphoserine intermediate, while formation of the hydroxide ion would be less feasible in the presence of an aryl substrate. Therefore, the second energy barrier results the highest for aryl phosphates, and the rate-determining step of the enzymatic mechanism becomes highly influenced by the pH of the media (at pH < 7.5 k_3 is rate-limiting; at pH > 7.5 k_4 is rate-limiting).[14−16]

Influence of the Metal Cation at the M3 Site. As regards the M3-Zn protein model, computational results were contrasted with experimental observations for the *E. coli* mutants K328H, D153H, and D153H/K328H, for which replacement of residues involved in binding metals to the M3 site was attained by site-specific mutagenesis.[65,66] Structural studies revealed that the octahedral magnesium binding site M3 of the wild-type protein had been converted to a tetrahedral zinc binding site in the mutant enzymes.[3,67] These mutants exhibited significantly lower hydrolytic activity than the wild-type enzyme for *p*-nitrophenylphosphate as substrate.[65,66] Thus, results in Table 1 are in good accordance with the reported kinetic assays, while the optimized geometry obtained for the M3 site in the M3-Zn protein model reproduces the X-ray crystallographic analysis.

For both M3-Mg and M3-Zn model enzymes, the hydroxyl group of nucleophilic Ser92 resulted ionized in the optimized structure of the Michaelis complex. Therefore, the activation of APs with Mg^{2+} at the M3 site would not be supported by a general base catalysis model. Hydrogen bonding between a nonbridging oxygen of the phosphate group and a water molecule coordinated to M3 was conserved during the whole enzymatic mechanism, with both Mg^{2+} or Zn^{2+} at M3. Furthermore, direct stabilization of the phosphoseryl group by complexation of one nonbridging oxygen atom with Zn_3 was also observed.

The present calculations suggest that the preferred Mg^{2+} octahedral coordination holds the active site in a catalytically more favorable configuration, resulting in activation of APs when this cation occupies the M3 site. This interpretation had been previously proposed on the basis of experimental evidence.[3,10,63] Moreover, these computations imply that the rearrangement of the active site because of a tetrahedral Zn^{2+} at M3 causes additional stabilization of the covalent phosphoser-

ine intermediate, consequently hindering the hydrolytic limiting step for aryl phosphate substrates.

Role of the Catalytic Residues. The catalytic mechanism of APs has been deduced from structural X-ray studies of *E. coli* AP.[4] Analysis of the optimized structures along the calculated reaction pathway allows further insights into the functions of the catalytic amino acids included in the protein model. Regarding the metal triad, Zn_1 assists both chemical steps by stabilizing the first leaving group and the inorganic phosphate final product (Steps 1 and 4 in Schemes 2 and 3); and it also activates the nucleophilic water for the hydrolytic Step 4 by decreasing its p*K*a to favor hydroxide ion formation. Zn_2 helps in positioning the phosphate monoester substrate for the Ser92 attack (Step1), and activates this residue for its nucleophilic function by stabilizing the alkoxide form. Moreover, Zn_2 stabilizes Ser92 as the leaving group in Step 4. The metal ion at the M3 site provides additional stabilization for the phosphate group; the influence of the metal identity has been discussed above.

The good conservation of the interatomic distances between the three metal cations upon free optimizations during the catalytic pathway, suggests that their ligand residues (Asp316, His320, His432, His358, Asp357, Asp42, Glu311, Ser155, as well as the nucleophilic Ser92) contribute to catalysis by maintaining the metal ions in place, in support of the hypothesis from mutagenesis studies.[68] In this regard, coordination of Asp42 to both M2 and M3 highlights the important interaction among the metal binding sites, as it has been proposed.[9]

Besides favoring the binding of the substrate within the active site, hydrogen-bonding interactions of the guanidinium group of Arg166 with the nonbridging phosphate oxygens stabilize the trigonal bipyramidal geometry of both TSs of the catalytic pathway, keeping the phosphoryl group in an optimal orientation. On the basis of experimental observations, it has been suggested that this residue preferentially stabilizes the TS relative to the covalently and noncovalently bound species.[62]

By interacting with water molecules within the active site, the acidic side-chain of Glu429 favors the formation of a hydrogen bonding network from this residue to the phosphate group of the covalent phosphoserine. Since one of these molecules is the nucleophilic water implicated in the crucial step of hydrolysis of the phosphoseryl intermediate, Glu429 affects the catalytic efficiency of the enzyme by providing an environment that reinforces the nucleophilic potency of this water molecule.

■ CONCLUDING REMARKS

The catalytic mechanism of PLAP was explored by quantum mechanical computations, using an active-site model constructed on the basis of an X-ray crystal structure of the enzyme. The reactions of hydrolysis of phenyl and methylphosphate, as models for aryl and alkyl phosphates, were investigated within the environment of the enzyme. Intermediates and TSs along the reaction pathway were optimized and characterized.

In accordance with experimental evidence,[14−17] computed values in this study indicate k_3 as rate-determining for the phenylphosphate substrate, whereas the chemical step of phosphorylation of the enzyme (k_2) yielded the highest activation barrier for methylphosphate. Hence, the computational results for both types of substrates are in good agreement with the experimental observations reported in the literature concerning the difference in rate-determining step among aryl and alkyl phosphates.

Regarding the factors determining this change in rate-limiting step, the difference in basicity between the corresponding leaving groups appears to be the main feature influencing the barrier height for the first chemical step (k_2). In this way, departure of a saturated alkoxide becomes rate-determining for alkyl phosphates, while this step is favored with a more stable aromatic alkoxide as the leaving group. In the second chemical step (k_3), the presence of the more basic methoxide anion would promote ionization of the Zn_1-coordinated water molecule to generate the nucleophilic hydroxide, facilitating the hydrolysis of the phosphoserine intermediate. On the other hand, formation of the hydroxide ion would be less feasible in the presence of an aryl substrate. Therefore, the second energy barrier results the highest for aryl phosphates, and the rate-limiting step of the enzymatic mechanism thus becomes highly influenced by the pH of the surrounding media, as it has been experimentally observed.[14−16]

The present computations suggest that PLAP increases the rate of hydrolysis by a factor of 2.4×10^{17} with methylphosphate as the substrate, and of 2.6×10^{16} for phenylphosphate. These observations are in good accordance with the catalytic proficiencies experimentally measured for APs.[60] Calculated activation barriers ended up being higher than those derived from assessed k_{cat}/K_M values, and consistent with those derived from k_{cat} values.

Results indicate that the preferred octahedral coordination of Mg^{2+} holds the active site in a catalytically more favorable configuration, resulting in activation of APs when Mg^{2+} occupies the M3 site. Moreover, the present calculations suggest that the rearrangement of the active site owing to a tetrahedral Zn^{2+} at M3 causes additional stabilization of the covalent phosphoserine intermediate, consequently hindering the hydrolytic limiting step for aryl phosphate substrates. These remarks are consistent with the lower activity of APs when Zn^{2+} replaces Mg^{2+} at the M3 site.[7−10,65,66]

Negligible modifications in the atomic coordinates of the amino acids comprising the PLAP model were observed during the course of the catalytic mechanism, implying the optimal organization of the active site for assisting the hydrolysis of phosphate monoesters. Analysis of the optimized structures along the calculated reaction pathway enabled to gain further insight into the functions of the catalytic residues included in the protein model.

■ ASSOCIATED CONTENT

Supporting Information

Selected stationary points for the M3-Zn enzyme model, and Cartesian coordinates for relevant optimized stationary points. This material is available free of charge via the Internet at http://pubs.acs.org.

■ AUTHOR INFORMATION

Corresponding Author

*E-mail: gborosky@fcq.unc.edu.ar; Tel: +54-351-535-3853.

Notes

The authors declare no competing financial interest.

■ ACKNOWLEDGMENTS

The author gratefully acknowledges financial support from Consejo Nacional de Investigaciones Científicas y Técnicas

(CONICET) and the Secretaría de Ciencia y Tecnología de la Universidad Nacional de Córdoba (Secyt-UNC).

REFERENCES

(1) McComb, R. B.; Bowers, G. N., Jr.; Posen, S. Measurement of Alkaline Phosphatase Activity. In *Alkaline Phosphatases*; Plenum Press: New York, 1979; pp 986−989.

(2) Kim, E. E.; Wyckoff, H. W. Structure of Alkaline Phosphatases. *Clin. Chim. Acta* **1990**, *186*, 175−178.

(3) Murphy, J. E.; Tibbitts, T. T.; Kantrowitz, E. R. Mutations at Positions 153 and 328 in *Escherichia coli* Alkaline Phosphatase Provide Insight Towards the Structure and Function of Mammalian and Yeast Alkaline Phosphatases. *J. Mol. Biol.* **1995**, *253*, 604−617.

(4) Kim, E. E.; Wyckoff, H. W. Reaction Mechanism of Alkaline Phosphatase Based on Crystal Structures: Two-Metal Ion Catalysis. *J. Mol. Biol.* **1991**, *218*, 449−464.

(5) Millán, J. L. *Mammalian Alkaline Phosphatases: From Biology to Applications in Medicine and Biotechnology*; Wiley-VCH Verlag GmbH & Co.: Weinheim, Germany, 2006; pp 1−322.

(6) Schwartz, J. H.; Lipmann, F. Phosphate Incorporation into Alkaline Phosphatase of *E. coli*. *Proc. Natl. Acad. Sci. U.S.A.* **1961**, *47*, 1996−2005.

(7) Anderson, R. A.; Bosron, W. F.; Kennedy, F. S.; Vallee, B. L. Role of Magnesium in *Escherichia coli* Alkaline Phosphatase. *Proc. Natl. Acad. Sci. U.S.A.* **1975**, *72*, 2989−2993.

(8) Xu, X.; Kantrowitz, E. R. Binding of Magnesium in a Mutant *Escherichia coli* Alkaline Phosphatase Changes the Rate-Determining Step in the Reaction Mechanism. *Biochemistry* **1993**, *32*, 10683−10691.

(9) Tibbitts, T. T.; Murphy, J. E.; Kantrowitz, E. R. Kinetic and Structural Consequences of Replacing the Aspartate Bridge by Asparagine in the Catalytic Metal Triad of *Escherichia coli* Alkaline Phosphatase. *J. Mol. Biol.* **1996**, *257*, 700−715.

(10) Hung, H.-C.; Chang, G.-G. Differentiation of the Slow-Binding Mechanism for Magnesium Ion Activation and Zinc Ion Inhibition of Human Placental Alkaline Phosphatase. *Protein Sci.* **2001**, *10*, 34−45.

(11) Holtz, K. M.; Kantrowitz, E. R. The Mechanism of the Alkaline Phosphatase Reaction: Insights from NMR, Crystallography and Site-specific Mutagenesis. *FEBS Lett.* **1999**, *462*, 7−11.

(12) Reid, T. W.; Wilson, I. B. *Escherichia coli* Alkaline Phosphatase. In *The Enzymes*; Boyer, P. D., Ed.; Academic Press: New York, 1971; Vol. *4*, pp 373−415.

(13) Coleman, J. E. Structure and Mechanism of Alkaline Phosphatase. *Annu. Rev. Biophys. Biomol. Struct.* **1992**, *21*, 441−483.

(14) Bloch, W.; Gorby, M. S. Catalytic Mechanism of *Escherichia coli* Alkaline Phosphatase: Resolution of Three Variants of the Acyl-Enzyme Mechanism. *Biochemistry* **1980**, *19*, 5008−5018.

(15) Gettins, P.; Coleman, J. E. 31P Nuclear Magnetic Resonance of Phosphoenzyme Intermediates of Alkaline Phosphatase. *J. Biol. Chem.* **1983**, *258*, 408−416.

(16) Hull, W. E.; Halford, S. E.; Gutfreund, H.; Sykes, B. D. Phosphorus-31 Nuclear Magnetic Resonance Study of Alkaline Phosphatase: The Role of Inorganic Phosphate in Limiting the Enzyme Turnover Rate at Alkaline pH. *Biochemistry* **1976**, *15*, 1547−1561.

(17) O'Brien, P. J.; Herschlag, D. Alkaline Phosphatase Revisited: Hydrolysis of Alkyl Phosphates. *Biochemistry* **2002**, *41*, 3207−3225.

(18) Hummer, C.; Millán, J. L. Gly429 is the Major Determinant of Uncompetitive Inhibition of Human Germ Cell Alkaline Phosphatase by *L*-leucine. *Biochem. J.* **1991**, *274*, 91−95.

(19) Le Du, M. H.; Stigbrand, T.; Taussig, M. J.; Ménez, A.; Stura, E. A. Crystal Structure of Alkaline Phosphatase from Human Placenta at 1.8 Å Resolution. *J. Biol. Chem.* **2001**, *276*, 9158−9165.

(20) Makiya, R.; Stigbrand, T. Placental Alkaline Phosphatase has a Binding Site for the Human Immunoglobulin-G Fc Portion. *Eur. J. Biochem.* **1992**, *205*, 341−345.

(21) Makiya, R.; Stigbrand, T. Placental Alkaline Phosphatase is Related to Human IgG Internalization in HEp2 Cells. *Biochem. Biophys. Res. Commun.* **1992**, *182*, 624−630.

(22) Stefaner, I.; Stefanescu, A.; Hunziker, W.; Fuchs, R. Expression of Placental Alkaline Phosphatase Does Not Correlate with IgG Binding, Internalization and Tanscytosis. *Biochem. J.* **1997**, *327*, 585−592.

(23) She, Q.-B.; Mukherjee, J. J.; Huang, J.; Crilly, K. S.; Kiss, Z. Growth Factor-like Effects of Placental Alkaline Phosphatase in Human Fetus and Mouse Embryo Fibroblasts. *FEBS Lett.* **2000**, *469*, 163−167.

(24) She, Q.-B.; Mukherjee, J. J.; Chung, T.; Kiss, Z. Placental Alkaline Phosphatase, Insulin, and Adenine Nucleotides or Adenosine Synergistically Promote Long-term Survival of Serum-starved Mouse Embryo and Human Fetus Fibroblasts. *Cell. Signal.* **2000**, *12*, 659−665.

(25) Lin, S.; Sartori, M. J.; Mezzano, L.; de Fabro, S. P. Placental Alkaline Phosphatase (PLAP) Enzyme Activity and Binding to IgG in Chagas' Disease. *Placenta* **2005**, *26*, 789−795 and references therein..

(26) Fishman, W. H.; Inglis, N. R.; Stolbach, L. L.; Krant, M. J. A Serum Alkaline Phosphatase Isoenzyme of Human Neoplastic Cell Origin. *Cancer Res.* **1968**, *36*, 935−938.

(27) Dempo, K.; Elliot, K. A. C.; Desmond, W.; Fishman, W. H. Demonstration of Gamma-glutamyl Transferase, Alkaline Phosphatase, CEA and HCG in Human Lung Cancer. *Oncodev. Biol. Med.* **1981**, *2*, 21−37.

(28) Nouwen, E. J.; Pollet, D. E.; Schelstraete, J. B.; Eerdekens, M. W.; Hänsch, C.; Van de Voorde, A.; De Broe, M. E. Human Placental Alkaline Phosphatase in Benign and Malignant Ovarian Neoplasia. *Cancer Res.* **1985**, *45*, 892−902.

(29) Nouwen, E. J.; Pollet, D. E.; Eerdekens, M. W.; Hendrix, P. G.; Briers, T. W.; De Broe, M. E. Immunohistochemical Localization of Placental Alkaline Phosphatase, Carcinoembryonic Antigen, and Cancer Antigen 125 in Normal and Neoplastic Human Lung. *Cancer Res.* **1986**, *46*, 866−876.

(30) Wick, M. R.; Swanson, P. E.; Manivel, J. C. Placental-like Alkaline Phosphatase Reactivity in Human Tumors: An Immunohistochemical Study of 520 Cases. *Hum. Pathol.* **1987**, *18*, 946−954.

(31) Borosky, G. L.; Lin, S. Computational Modeling of the Catalytic Mechanism of Human Placental Alkaline Phosphatase (PLAP). *J. Chem. Inf. Model.* **2011**, *51*, 2538−2548.

(32) Morris, G. M.; Huey, R.; Lindstrom, W.; Sanner, M. F.; Belew, R. K.; Goodsell, D. S.; Olson, A. J. AutoDock4 and AutoDockTools4: Automated Docking with Selective Receptor Flexibility. *J. Comput. Chem.* **2009**, *30*, 2785−2791.

(33) Blomberg, M. R. A.; Borowski, T.; Himo, F.; Liao, R.-Z.; Siegbahn, P. E. M. Quantum Chemical Studies of Mechanisms for Metalloenzymes. *Chem. Rev.* **2014**, *114*, 3601−3658.

(34) Siegbahn, P. E. M.; Himo, F. The Quantum Chemical Cluster Approach for Modeling Enzyme Reactions. *WIREs Comp. Mol. Sci.* **2011**, *1*, 323−336 and references therein..

(35) Siegbahn, P. E. M.; Himo, F. Recent Developments of the Quantum Chemical Cluster Approach for Modeling Enzyme Reactions. *J. Biol. Inorg. Chem.* **2009**, *14*, 643−451 and references therein..

(36) Dapprich, S.; Komáromi, I.; Byun, K. S.; Morokuma, K.; Frisch, M. J. A New ONIOM Implementation in Gaussian98. Part I. The Calculation of Energies, Gradients, Vibrational Frequencies and Electric Field Derivatives. *J. Mol. Struct. (THEOCHEM)* **1999**, *461*−*462*, 1−21.

(37) Frisch, M. J.; Trucks, G. W.; Schlegel, H. B.; Scuseria, G. E.; Robb, M. A.; Cheeseman, J. R.; Scalmani, G.; Barone, V.; Mennucci, B.; Petersson, G. A. et al. *Gaussian 09*, revision A.01; Gaussian, Inc.: Wallingford, CT, 2009.

(38) Becke, A. D. Density-functional Thermochemistry. III. The Role of Exact Exchange. *J. Chem. Phys.* **1993**, *98*, 5648−5652.

(39) Lee, C.; Yang, W.; Parr, R. G. Development of the Colle−Salvetti Correlation-Energy Formula into a Functional of the Electron Density. *Phys. Rev. B* **1988**, *37*, 785−789.

(40) Miehlich, B.; Savin, A.; Stoll, H.; Preuss, H. Results Obtained with the Correlation Energy Density Functionals of Becke and Lee, Yang and Parr. *Chem. Phys. Lett.* **1989**, *157*, 200−206.

(41) Chai, J.-D.; Head-Gordon, M. Long-Range Corrected Hybrid Density Functionals with Damped Atom−Atom Dispersion Corrections. *Phys. Chem. Chem. Phys.* **2008**, *10*, 6615−6620.
(42) Stewart, J. J. P. Optimization of Parameters for Semiempirical Methods. I. Method. *J. Comput. Chem.* **1989**, *10*, 209−220.
(43) Stewart, J. J. P. Optimization of Parameters for Semiempirical Methods V: Modification of NDDO Approximations and Application to 70 Elements. *J. Mol. Model.* **2007**, *13*, 1173−1213.
(44) Cancès, E.; Mennucci, B.; Tomasi, J. A New Integral Equation Formalism for the Polarizable Continuum Model: Theoretical Background and Applications to Isotropic and Anisotropic Dielectrics. *J. Chem. Phys.* **1997**, *107*, 3032−3041.
(45) Mennucci, B.; Tomasi, J. Continuum Solvation Models: A New Approach to the Problem of Solute's Charge Distribution and Cavity Boundaries. *J. Chem. Phys.* **1997**, *106*, 5151−5158.
(46) Mennucci, B.; Cancès, E.; Tomasi, J. Evaluation of Solvent Effects in Isotropic and Anisotropic Dielectrics and in Ionic Solutions with a Unified Integral Equation Method: Theoretical Bases, Computational Implementation, and Numerical Applications. *J. Phys. Chem. B* **1997**, *101*, 10506−10517.
(47) Tomasi, J.; Mennucci, B.; Cancès, E. The IEF Version of the PCM Solvation Method: An Overview of a New Method Addressed to Study Molecular Solutes at the QM Ab Initio Level. *J. Mol. Struct. (THEOCHEM)* **1999**, *464*, 211−226.
(48) Llinas, P.; Stura, E. A.; Ménez, A.; Kiss, Z.; Stigbrand, T.; Millán, J. L.; Le Du, M. H. Structural Studies of Human Placental Alkaline Phosphatase in Complex with Functional Ligands. *J. Mol. Biol.* **2005**, *350*, 441−451.
(49) Stec, B.; Holtz, K. M.; Kantrowitz, E. R. A Revised Mechanism for the Alkaline Phosphatase Reaction Involving Three Metal Ions. *J. Mol. Biol.* **2000**, *299*, 1303−1311.
(50) Zalatan, J. G.; Fenn, T. D.; Herschlag, D. Comparative Enzymology in the Alkaline Phosphatase Superfamily to Determine the Catalytic Role of an Active-Site Metal Ion. *J. Mol. Biol.* **2008**, *384*, 1174−1189.
(51) Jencks, W. P.; Regenstein, J. Ionization Constants of Acids and Bases. In *Handbook of Biochemistry and Molecular Biology*; Fasman, G. D., Ed.; CRC Press: Cleveland, OH, 1976; pp 305−351.
(52) Geometry optimizations were performed in gas phase, where the separation of charges is avoided, while in a continuum polarized model it is favored. Consequently, optimization of geometries in a polarized continuum may yield different results, especially regarding the spontaneous proton transfers mentioned in the text. PCM optimizations with more substrates are currently ongoing in a subsequent study.
(53) Holtz, K. M.; Stec, B.; Kantrowitz, E. R. A Model of the Transition State in the Alkaline Phosphatase Reaction. *J. Biol. Chem.* **1999**, *274*, 8351−8354.
(54) Duarte, F.; Amrein, B. A.; Kamerlin, S. C. L. Modeling Catalytic Promiscuity in the Alkaline Phosphatase Superfamily. *Phys. Chem. Chem. Phys.* **2013**, *15*, 11160−11177 and references therein..
(55) Hou, G.; Cui, Q. Stabilization of Different Types of Transition States in a Single Enzyme Active Site: QM/MM Analysis of Enzymes in the Alkaline Phosphatase Superfamily. *J. Am. Chem. Soc.* **2013**, *135*, 10457−10469.
(56) Roe, R. R.; Pang, Y.-P. Zinc's Exclusive Tetrahedral Coordination Governed by its Electronic Structure. *J. Mol. Model.* **1999**, *5*, 134−140.
(57) The classical transition-state theory expresses the rate constant for a reaction as $k = (k_B T/h) \exp(-\Delta G/RT)$, in which k_B is the Boltzmann constant, R is the gas constant, T is the absolute temperature, h is the Planck constant, and ΔG is the free energy of activation.
(58) Ribeiro, A. J. M.; Alberto, M. E.; Ramos, M. J.; Fernandes, P. A.; Russo, N. The Catalytic Mechanism of Protein Phosphatase 5 Established by DFT Calculations. *Chem.—Eur. J.* **2013**, *19*, 14081−14089 and references therein..
(59) Lad, C.; Williams, N. H.; Wolfenden, R. The Rate of Hydrolysis of Phosphomonoester Dianions and the Exceptional Catalytic Proficiencies of Protein and Inositol Phosphatases. *Proc. Natl. Acad. Sci. U.S.A.* **2003**, *100*, 5607−5610.
(60) O'Brien, P. J.; Herschlag, D. Functional Interrelationships in the Alkaline Phosphatase Superfamily: Phosphodiesterase Activity of *Escherichia coli* Alkaline Phosphate. *Biochemistry* **2001**, *40*, 5691−5699.
(61) Bale, J. R.; Huang, C. Y.; Chock, P. B. Transient Kinetic Analysis of the Catalytic Cycle of Alkaline Phosphatase. *J. Biol. Chem.* **1980**, *255*, 8431−8436.
(62) O'Brien, P. J.; Lassila, J. K.; Fenn, T. D.; Zalatan, J. G.; Herschlag, D. Arginine Coordination in Enzymatic Phosphoryl Transfer: Evaluation of the Effect of Arg166 Mutations in *Escherichia coli* Alkaline Phosphatase. *Biochemistry* **2008**, *47*, 7663−7672.
(63) Chen, S.-L.; Liao, R.-Z. Phosphate Monoester Hydrolysis by Trinuclear Alkaline Phosphatase; DFT Study of Transitions States and Reaction Mechanism. *ChemPhysChem* **2014**, *15*, 2321−2330.
(64) Spitznagel, G. W.; Clark, T.; Schleyer, P. v. R.; Hehre, W. J. An Evaluation of the Performance of Diffuse Function-Augmented Basis Sets for Second Row Elements, Na−Cl. *J. Comput. Chem.* **1987**, *8*, 1109−1116 and references therein..
(65) Janeway, C. M. L.; Xu, X.; Murphy, J. E.; Chaidaroglou, A.; Kantrowitz, E. R. Magnesium in the Active Site of *Escherichia coli* Alkaline Phosphatase is Important for Both Structural Stabilization and Catalysis. *Biochemistry* **1993**, *32*, 1601−1609.
(66) Wojciechowski, C. L.; Kantrowitz, E. R. Altering of the Metal Specificity of *Escherichia coli* Alkaline Phosphatase. *J. Biol. Chem.* **2002**, *277*, 50476−50481.
(67) Murphy, J. E.; Xu, X.; Kantrowitz, E. R. Conversion of a Magnesium Binding Site Into a Zinc Binding Site by a Single Amino Acid Substitution in *Escherichia coli* Alkaline Phosphatase. *J. Biol. Chem.* **1993**, *268*, 21497−21500.
(68) Kozlenkov, A.; Manes, T.; Hoylaerts, M. F.; Millán, J. L. Function Assignment to Conserved Residues in Mammalian Alkaline Phosphatases. *J. Biol. Chem.* **2002**, *277*, 22992−22999.